

Polarization-resolved sensing with tilted fiber Bragg gratings: theory and limits of detection

This content has been downloaded from IOPscience. Please scroll down to see the full text.

2015 J. Opt. 17 085601

(<http://iopscience.iop.org/2040-8986/17/8/085601>)

View [the table of contents for this issue](#), or go to the [journal homepage](#) for more

Download details:

IP Address: 134.117.97.252

This content was downloaded on 22/03/2016 at 16:56

Please note that [terms and conditions apply](#).

Polarization-resolved sensing with tilted fiber Bragg gratings: theory and limits of detection

Aliaksandr Bialiyeu¹, Anatoli Ianoul² and Jacques Albert¹

¹Department of Electronics, Carleton University, 1125 Colonel By Drive, Ottawa, ON K1S5B6, Canada

²Department of Chemistry, Carleton University, 1125 Colonel By Drive, Ottawa, ON K1S5B6, Canada

E-mail: alexbeliaev@gmail.com

Received 3 February 2015, revised 23 May 2015

Accepted for publication 27 May 2015

Published 20 July 2015



CrossMark

Abstract

Polarization based sensing with tilted fiber Bragg grating (TFBG) sensors is analysed theoretically by two alternative approaches. The first method is based on tracking the grating transmission for two orthogonal states of linear polarized light that are extracted from the measured Jones matrix or Stokes vectors of the TFBG transmission spectra. The second method is based on the measurements along the system principle axes and polarization dependent loss (PDL) parameter, also calculated from measured data. It is shown that the frequent crossing of the Jones matrix eigenvalues as a function of wavelength leads to a non-physical interchange of the calculated principal axes; a method to remove this unwanted mathematical artefact and to restore the order of the system eigenvalues and the corresponding principal axes is provided. A comparison of the two approaches reveals that the PDL method provides a smaller standard deviation and therefore lower limit of detection in refractometric sensing. Furthermore, the polarization analysis of the measured spectra allows for the identification of the principal states of polarization of the sensor system and consequentially for the calculation of the transmission spectrum for any incident polarization state. The stability of the orientation of the system principal axes is also investigated as a function of wavelength.

Keywords: fiber optics sensors, fiber Bragg gratings, polarization-selective devices, ellipsometry and polarimetry

1. Introduction

Polarization-based sensing is crucial for various types of optical sensors, in particular for stress analysis, plasmon-mediated sensing, and sensing of anisotropic media or other forms of perturbations [1–4]. In the particular case of waveguide-type sensors (including optical fibers), it is possible to interrogate the device optical properties with polarized light but in general this requires very careful alignment and control of the input polarization, which is relatively easy in waveguides but not so much in conventional fibers. In the latter case for instance, polarization information can be crucial to optimize both the sensitivity and limit of detection of metal-coated fiber refractometric sensors for biochemical applications [5, 6]. Here we describe a data analysis method that provides a full characterization of the polarization-resolved

optical transmission state of any sensor system based on measurements of the wavelength dependence of the Jones matrix with an optical vector analyser ('OVA', i.e. in our case the OVA 5000 from Luna Technologies Inc.). The OVA measures the transmission amplitude and phase (or reflection) of an optical system as a function of polarization and wavelength and provides the Jones matrix elements for each wavelength. We use a standard tilted fiber Bragg grating (TFBG) refractometric sensor as a test system for demonstrating the new approach. TFBGs can be used to measure the refractive index of bulk media or of coatings because they couple light from the core guided mode to modes guided by the cladding, and because the wavelengths at which these couplings occur depend on the external refractive index. The results confirm that the polarization dependent loss parameter (PDL) of the system provides a smaller standard deviation

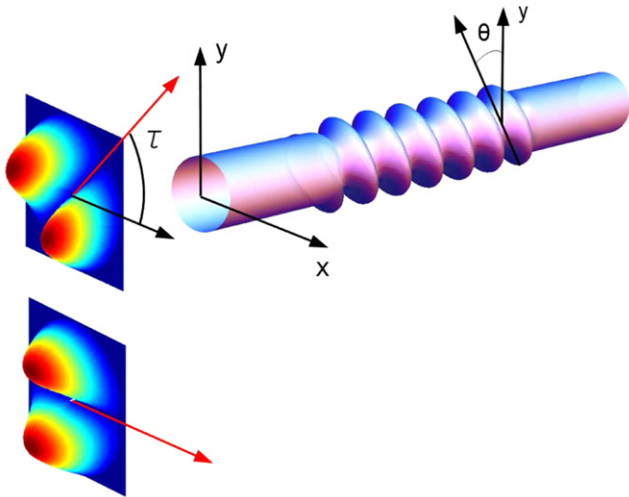


Figure 1. The schematic representation of TFBG grating and the incident linearly polarized core mode HE_{11} (only E_ρ component of the core mode is shown). The core mode is rotated about the optical device axis by some angle τ . The grating is tilted by θ angle about the \hat{x} axis, and hence the principal axes of the fiber device are \hat{x} and \hat{y} . The geometrical axis (not shown) used in the text refers to the arbitrary orientation of the zero angle of the polarization of the spectral interrogation system.

(and hence better limit of detection) than the transmission spectra extracted along the principal axes, as initially observed empirically in [6].

It is known that TFBGs have strong polarization-dependent properties [5, 7, 8, 10] due to the tilt of the grating planes which breaks the cylindrical symmetry of the fiber and strongly impacts the magnitude of the coupling coefficients between the incident HE_{11} core mode and the cladding modes of various polarizations (**TE**, **TM**, **HE**, **EH** modes) excited by the grating [11, 12], as it is shown schematically in figure 1.

In particular, for a grating tilted by an angle θ in the reference $y-z$ plane and a linearly polarized input core mode whose polarization is rotated by an arbitrary angle τ about the z axis (a most general occurrence in optical fibers that are not polarization preserving), the coupling to individual cladding modes will depend strongly on both θ and τ . It has been further demonstrated recently that high order cladding modes of the **EH** and **TM** families have radially polarized evanescent fields around the fiber cladding while **HE/TE** modes are azimuthally polarized [10]. This is important because in many sensing applications (or other forms of interactions between cladding guided light and coatings or external media, such as nonlinear switching [13], or four wave mixing [14] applications), the state of polarization of the evanescent field can be a determining factor. This is most easily seen for metallic coatings whose boundary conditions depend strongly on the polarization of the incident electric field relative to the plane of the boundary [6, 8]. It was also demonstrated in [10] that only radially polarized cladding modes are excited by TFBGs when the input core mode is linearly polarized along the tilt plane (i.e. along y), while the orthogonal input polarization (along x) generates only azimuthally polarized cladding modes. The

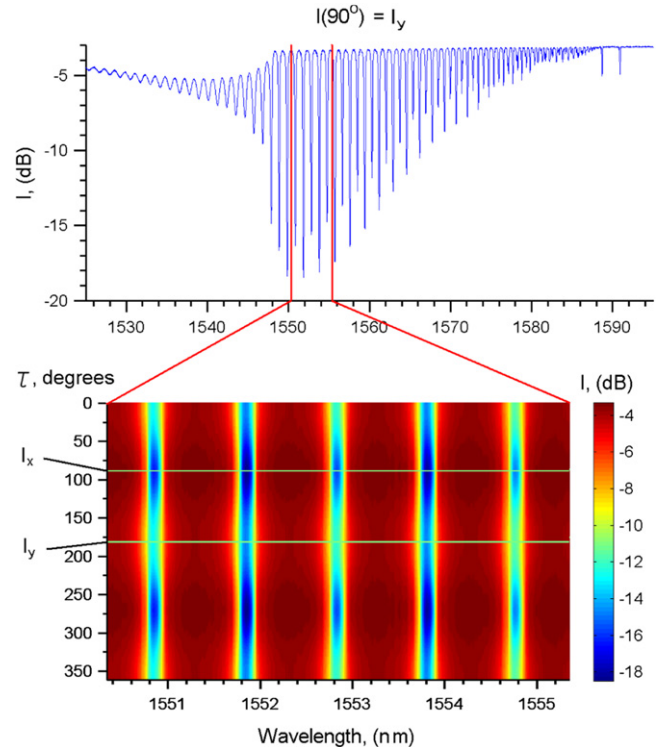


Figure 2. A typical TFBG transmission spectrum for linearly polarized light, and series of spectra obtained by rotating a linear polarizer about the optical axis are shown as a density plot.

effect of the input mode polarization can be observed by measuring optical transmission spectra with a polarizer inserted between the light source and the grating [9, 15]. A typical series of spectra measured at various angles of linearly polarized incident light is shown in figure 2 for a 1 cm long TFBG immersed in water. The optical device was made in a standard non-polarization-maintaining telecom single mode optical fiber (Corning SMF-28), in which a uniform 1 cm-long TFBG grating with a tilt angle of 6° was inscribed. The measurement set-up in this case consisted of a micron optics si720 FBG interrogator (based on a tunable laser with a photo detector).

It is clear from figure 2 that there are two orthogonal states of transmission, oriented at 90° relative to each other, where the spectrum has well-defined extrema. We can therefore find the polarizer angles for which **TE** and **TM** modes are excited *a posteriori* without prior knowledge of the actual orientation of the tilt plane. However this is often impractical, especially if the device under test has to be moved between measurements, thereby potentially altering the light polarization orientation between the polarizer and the TFBG. This method also assumes that the principal axes of the device under test are the same at all wavelengths, which is not totally accurate as shown at the end of section 2. A much more practical, rapid, and accurate method to interrogate such devices is to use an OVA to get the Jones matrix elements at each wavelength and to use the information to calculate the full set of polarization properties of the system, including the transmission along the chosen geometrical axes (I_x and I_y in

figure 2) as well as the transmission along the system principal axes and PDL spectrum. How this is done is presented in the next section.

2. Measurements along principal axes of an optical system

In this section we review the PDL technique and provide an approach to study the system transmission spectrum along its principal axes.

A linear optical system can be represented in terms of the 2×2 Jones matrix $[J]$ connecting the incident and transmitted electric field vectors [16]:

$$\vec{E}_{out} = [J]\vec{E}_{in}. \quad (1)$$

In practice, the transmission spectrum of a device under test is usually characterized by two major parameters: a polarization-independent parameter called the insertion loss $I(\lambda)$ and the PDL parameter (λ) , both measured as a function of the free space wavelength λ . To extract these parameters from the Jones matrix, a hermitian matrix $[H]$ has to be constructed first

$$[H] = [J]^\dagger [J]. \quad (2)$$

Next, carrying out the eigen decomposition of the $[H]$ matrix

$$[H] = [U][\Lambda][U]^T \quad (3)$$

allows us to find a diagonal matrix $[\Lambda]$ containing the eigenvalues ρ_1 and ρ_2 of the $[H]$ matrix.

Alternatively, the singular value decomposition (SVD) of the Jones matrix can be computed [17]:

$$[J] = [U][\Sigma][V]^T, \quad (4)$$

where the diagonal matrix $[\Sigma]$ contains two singular values σ_1 and σ_2 such that $\rho_1 = \sigma_1^2$ and $\rho_2 = \sigma_2^2$, due to the fact that $[H] = [J]^\dagger [J]$.

The matrix $[U] = (\vec{u}_1, \vec{u}_2)$ resulting from the SVD contains two orthogonal vectors corresponding to ρ_1 and ρ_2 eigenvalues, and these eigenvectors correspond to the device response when the electric field vector \vec{E} is aligned with the system principal axes, i.e. $\vec{E} \parallel \vec{u}_k$ of the system (where k is an index = 1, 2). The eigenvalues $\rho_k = \sigma_k^2$ can be interpreted as the observable transmission loss for the corresponding incident polarizations. The other matrix $[V] = (\vec{v}_1, \vec{v}_2)$ results from the SVD algorithm but it is not used in the current analysis. The principal axes \vec{u}_1, \vec{u}_2 of an arbitrary fiber device are shown schematically in figure 3. The angle ϕ corresponds to the rotation between the arbitrarily selected frame of reference (x, y) and the principal axes defined by \vec{u}_1, \vec{u}_2 .

Having the singular values of the Jones matrix $[J]$ or eigenvalues of $[H] = [J]^\dagger [J]$ matrix allow for the computation of the insertion loss, which is the average loss over all

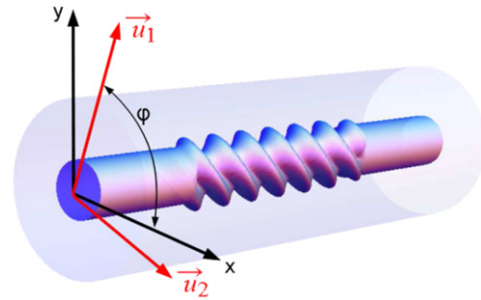


Figure 3. TFBG with geometrical \hat{x}, \hat{y} axes and principal system axes \vec{u}_1, \vec{u}_2 measured at some wavelength λ .

possible polarizations, as follows [17]

$$\begin{aligned} I_{out} &= \langle \vec{E}_{out} | \vec{E}_{out} \rangle = \langle \vec{E}_{in} | [J]^\dagger [J] | \vec{E}_{in} \rangle \\ &= \langle \vec{E}'_{in} | \Lambda | \vec{E}'_{in} \rangle = \frac{\rho_1 + \rho_2}{2} I_{in}. \end{aligned} \quad (5)$$

Which can be re-formulated in the more frequently used dB scale as:

$$\frac{I_{out}}{I_{in}} = 10 \log_{10} \frac{\rho_1 + \rho_2}{2}, \quad (6)$$

here, the scalar product is denoted in accordance with Dirac's bracket notation. Similarly, the PDL, which is the magnitude of the difference between the maximum and minimum device transmission over all possible input polarization actually corresponds to the difference in the loss measured along the system principal axes \vec{u}_1 and \vec{u}_2 . It is defined as follows:

$$PDL = 10 \left| \log_{10} \frac{\rho_1}{\rho_2} \right|. \quad (7)$$

Alternatively we can introduce a polarization parameter with a linear scale [8, 9]:

$$P = \frac{|\rho_1 - \rho_2|}{\rho_1 + \rho_2}. \quad (8)$$

These concepts are now applied to a measured real data set similar to the one shown in figure 2, but now made up of the amplitudes and phases of the Jones matrix elements at each measured wavelength, obtained by an OVA. In addition to the eigenvalues of the system transmission matrix (a subset of the data is plotted as a function of wavelength in figure 4), we can also find the angle of rotation (ϕ) of the principal axes about the device optical axis (z) and plot it as a function of wavelength (bottom frame of figure 4). From the mathematical point of view, both eigenvalues are roots of quadric polynomial and ordered arbitrary, usually in descending order: this is why ρ_1 is always larger than ρ_2 in figure 4(a), hence the eigenstates are interchanged when they cross. Because of this effect, the corresponding eigenvectors are interchanged as well, therefore the angle ϕ experiences $\pi/2$ shifts at the crossing points, as shown on the bottom panel of figure 4(a). Therefore, a strategy for restoring the individual

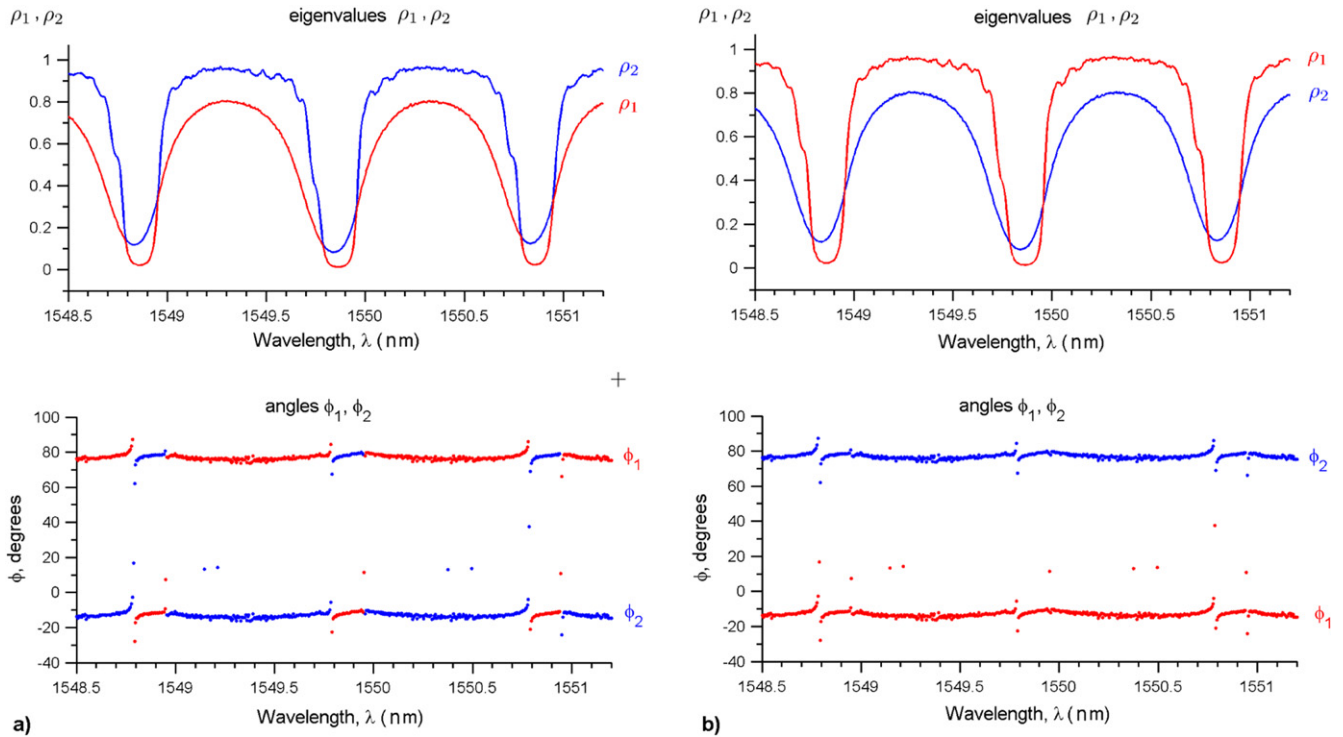


Figure 4. Eigenvalues ρ_1 and ρ_2 and the angle ϕ between the geometrical axes of the system \hat{x} , \hat{y} and the coordinate system defined by the principal axes \vec{u}_1 , \vec{u}_2 , before (a) and after (b) the eigenvalues were reordered. (The data was measured with the OVA.)

transmission spectra along the principal axes is to interchange the eigenvalues and principal axes every time the $\phi = \pi/2$ jumps are detected (automatically by the data processing algorithm).

The result of such reordering is shown figure 4(b). Now the transmission spectrum corresponds to linearly polarized light with its electric field vector aligned with each principal axis of the system and the rotation angle jumps are eliminated.

In general, the principal axes of an optical system are not necessarily fixed with respect to a reference frame but may depend on the wavelength, as shown in figure 5 for a TFBG sensor. Indeed, by changing the optical frequency it is expected that an optical system would operate differently. The global behaviour of the principal axes, along the whole operational range of the TFBG sensor, is shown in figure 5(b), and the corresponding insertion loss in figure 5(a). To remove the noise only the points at which the difference between eigenvalues is noticeable ($|\rho_2 - \rho_1| > 0.05$) are plotted. The noise arises from the fact, that at the points of eigenvalues crossing the transmission matrix become degenerate, as the eigenvectors are not well defined, and oscillate rapidly with respect to the geometrical axis, as it can be seen from figure 5(b) at the points of crossing.

Figure 5(b) shows that the system possesses significant polarization asymmetry, or birefringence, in the wavelength range $\lambda \in [1545-1575]$. Although the principal axes are globally stable, near 75° relative to the reference frame of the OVA interrogation system, locally they experience small oscillations, of about 8° about the optical axis. These

oscillations are related to the resonances observed in the spectrum (figure 5(a), and reflect a wavelength dependent birefringence.

We also note the observed alternation between the peaks (figure 5(a), which can be explained by the fact that the alternating peaks have different azimuthal symmetries and polarizations [11].

3. Extracting transmission spectra for light polarized in an arbitrary direction from the Jones matrix or the Stokes vector data

In this section we describe an approach allowing to extract the transmission loss spectra for light that is linearly polarized in any direction, which may be a useful predictive tool for device performance under real life conditions without the need for an external polarizer.

3.1. The Jones matrix analysis

The Jones matrix of an optical device under test connected to a linear polarizer is given by:

$$[J_{\text{dev+pol}}] = [J_{\text{dev}}][J_{\text{pol}}]. \quad (9)$$

Here $[J_{\text{dev}}]$ is Jones matrix of a device measured by an optical vector analyzer and $[J_{\text{pol}}]$ is the Jones matrix of a linear polarizer, oriented at an arbitrary angle theta relative to the

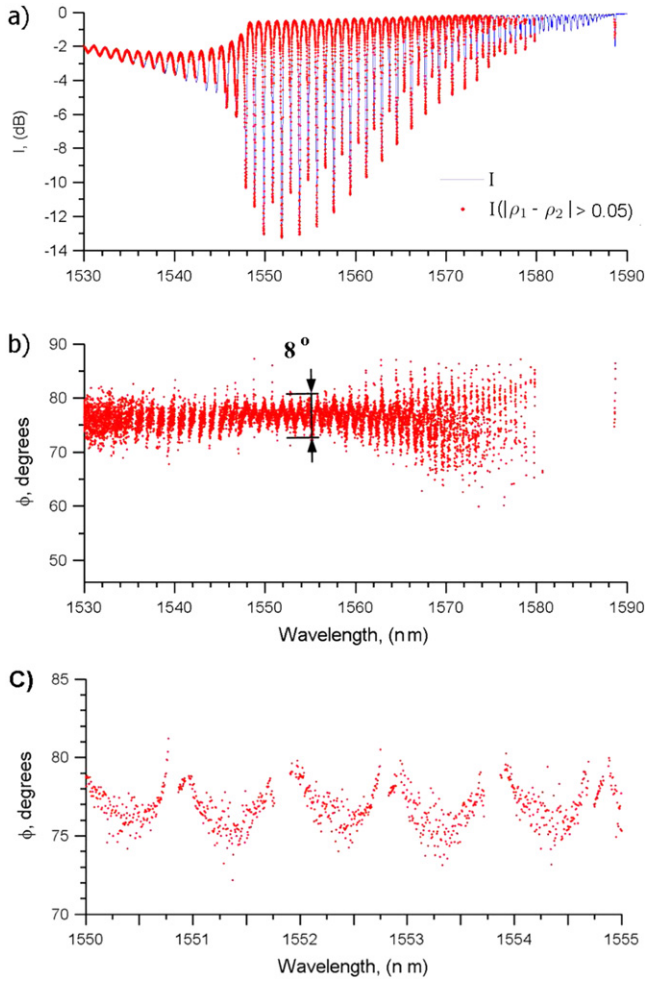


Figure 5. Rotation of the principal axes of TFBG device as a function of optical wavelength, (a) the whole spectrum of insertion loss $I(\lambda)$ shown in blue and noise free regions with $|\rho_2 - \rho_1| > 0.05$ are shown in red, (b) global behaviour of the principal axes, (c) zooming on a particular spectral region.

system frame of reference given by:

$$[J_{\text{pol}}(\theta)] = \begin{bmatrix} \cos^2(\theta) & \cos(\theta)\sin(\theta) \\ \sin(\theta)\cos(\theta) & \sin^2(\theta) \end{bmatrix}, \quad (10)$$

Thus, on optical device with a known Jones matrix $[J_{\text{dev}}]$, connected to a linear polarizer rotated by θ angle, is described by the following Jones matrix:

$$[J_{\text{dev+pol}}(\theta)] = [J_{\text{dev}}] \begin{bmatrix} \cos^2(\theta) & \cos(\theta)\sin(\theta) \\ \sin(\theta)\cos(\theta) & \sin^2(\theta) \end{bmatrix}. \quad (11)$$

And finally the average transmission spectrum $I(\theta, \lambda)$, for a given angle θ of the linear polarizer, can be computed as

$$I(\theta, \lambda) = 10 \log_{10} \frac{\rho_1(\theta, \lambda) + \rho_2(\theta, \lambda)}{2}, \quad (12)$$

where $\rho_1(\theta, \lambda)$ and $\rho_2(\theta, \lambda)$ are the eigenvalues of $H(\theta, \lambda) = [J_{\text{dev+pol}}(\theta, \lambda)]^\dagger [J_{\text{dev+pol}}(\theta, \lambda)]$ matrix.

3.2. The Stokes vector analysis

In the cases where the phase information obtained with a vector analyzer is not available, we provide here an alternative approach to calculating the response of a device to arbitrarily oriented linearly polarized light using the Stokes vector of the system. The Stokes vector can be measured with a conventional spectral measurement system to which a polarization controller is added or with a dedicated instrument, such as the JDS Uniphase SWS-OMNI-2 system.

A beam of light can be completely described by four parameters [18, 19], represented in the form of the Stokes vector:

$$\vec{S} = \begin{pmatrix} S_0 \\ S_1 \\ S_2 \\ S_3 \end{pmatrix} = \begin{pmatrix} I(0^\circ) + I(90^\circ) \\ I(0^\circ) - I(90^\circ) \\ I(45^\circ) - I(135^\circ) \\ I_{\text{rhs}} - I_{\text{lhs}} \end{pmatrix}, \quad (13)$$

here $I(\theta)$ is the measured power transmission coefficient of the light polarized in the direction defined by the angle θ in the plane perpendicular to the direction of light propagation, and I_{rhs} , I_{LHC} are the coefficients for right- and left-handed circular polarized light, respectively.

Since the Stokes parameters are dependent upon the choice of axes, they can be transformed into a different coordinate system with a rotation matrix $[R]$

$$[R(\theta)] = \begin{bmatrix} \cos(\theta) & -\sin(\theta) \\ \sin(\theta) & \cos(\theta) \end{bmatrix}, \quad (14)$$

Considering that a second coordinate system is obtained by rotating the original coordinate system about the direction of light propagation on the angle θ , we can write [20]

$$\vec{S}'(\theta) = [R(\theta)]\vec{S}, \quad (15)$$

or

$$\begin{pmatrix} S'_0 \\ S'_1 \\ S'_2 \\ S'_3 \end{pmatrix} = \begin{bmatrix} 1 & 0 & 0 & 0 \\ 0 & \cos(2\theta) & \sin(2\theta) & 0 \\ 0 & -\sin(2\theta) & \cos(2\theta) & 0 \\ 0 & 0 & 0 & 1 \end{bmatrix} \begin{pmatrix} S_0 \\ S_1 \\ S_2 \\ S_3 \end{pmatrix} = \begin{pmatrix} S_0 \\ S_1 \cos(2\theta) + S_2 \sin(2\theta) \\ -S_1 \sin(2\theta) + S_2 \cos(2\theta) \\ S_3 \end{pmatrix}, \quad (16)$$

Now considering that

$$\begin{aligned} I(0^\circ) + I(90^\circ) &= S_0, \\ I(0^\circ) - I(90^\circ) &= S_1 \cos(2\theta) + S_2 \sin(2\theta), \end{aligned} \quad (17)$$

we conclude that the transmission loss spectra along the two orthogonal axes, rotated by the angle θ with respect to the original system of measurements, are given by the following

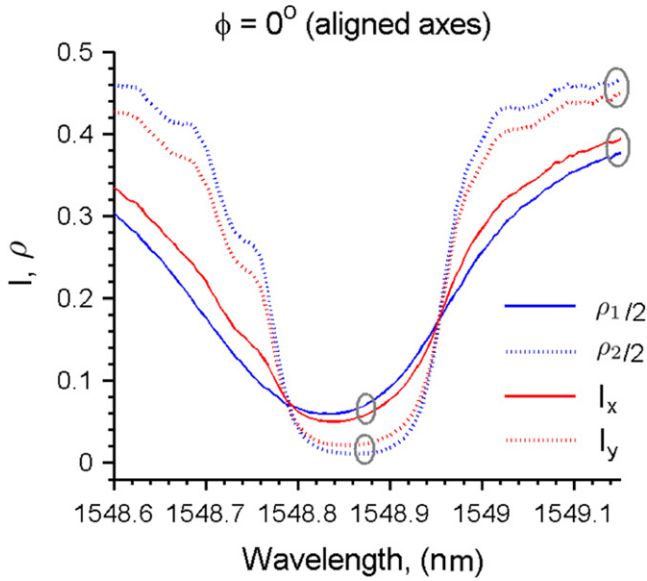


Figure 6. Transmission losses along TFBG system principal axes and its geometrical axes for perfectly aligned coordinate systems $\phi = 0^\circ$.

expressions:

$$I_x(\theta, \lambda) = \frac{1}{2}(S_o(\lambda) + S_1(\lambda)\cos(2\theta) + S_2(\lambda)\sin(2\theta)),$$

$$I_y(\theta, \lambda) = \frac{1}{2}(S_o(\lambda) - S_1(\lambda)\cos(2\theta) - S_2(\lambda)\sin(2\theta)). \quad (18)$$

Hence, if the Stokes vector is known in one coordinate system, the transmission spectrum of linearly polarized light with the electric field \vec{E} aligned along an arbitrary angle θ , can be recovered.

4. Comparison between measurements along the geometrical and principal axes

The last results show that the transmission spectra of light linearly polarized along any direction in the transverse plane of the optical axis can be computed from the Jones matrix or from the Stokes vector, in addition to the possibility of measuring it directly by rotating a polarizer, as shown in figure 2. In particular, the transmission spectra of light linearly polarized along the system principal axes can be extracted from the Jones matrix and compared to the direct measurement with a polarizer. Figure 6 shows a comparison between the direct measurement of one resonance, obtained by aligning the polarizer along the average direction of the principal axes (for a given spectrum), and the eigenstate spectra obtained from the Jones matrix. The small difference in the two results comes from the aforementioned wavelength dependent oscillation of the principal axes (which cannot be compensated for in the direct measurement), and to a possible slight change in polarization state between polarizer and the grating (since a non-polarization maintaining fiber is used). The following section will demonstrate that in spite of this small inaccuracy, the parameters extracted from the Jones

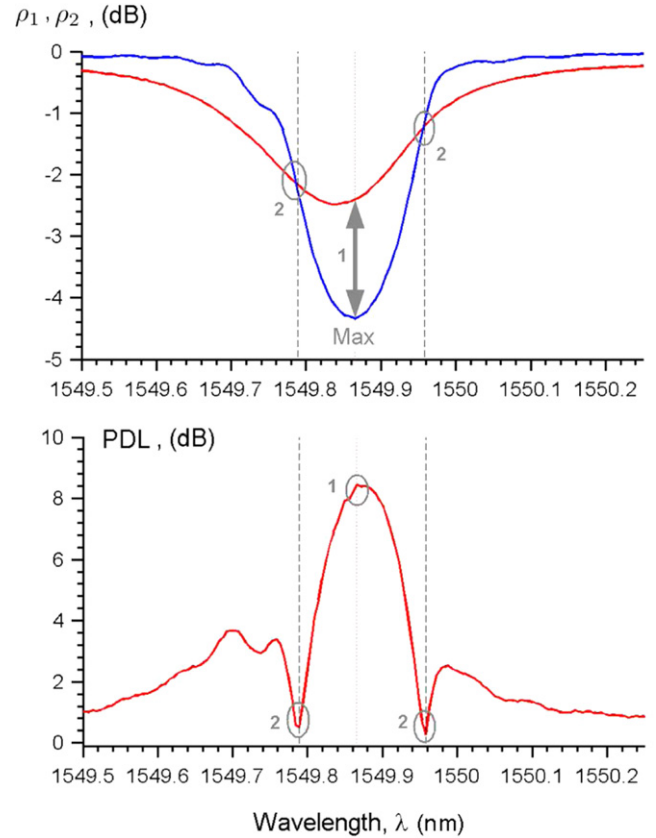


Figure 7. Two eigenvalue spectra (individual transmission along the principal axes) and corresponding polarization dependent loss (PDL) parameter. The peak in PDL spectrum is denoted by '1' and zeros by '2'. Here the more common dB scale is used.

matrix data provide excellent spectral sensitivity results for refractometric sensing.

5. Polarization-based detection of small refractive index changes with TFBG sensors

In this section we investigate which polarization-based measurement techniques provide the best signal-to-noise ratio when TFBG sensors are used to detect small refractive index changes, and use the special case of a TFBG coated with silver nanowires (as described in [8]). This choice is made because the polarization dependence of waveguide-type sensors is much enhanced when metal coatings are used. As indicated earlier, the interaction of guided waves with metal interfaces depends strongly on whether the electric fields of the waves are tangential or normal to the metal boundary. It was further mentioned that when the core-guided input light of a TFBG is linearly polarized along the principal axes, the electric fields of high order cladding modes are either tangential or radial (hence normal) to the cladding boundary. To be precise, y-polarized input light (corresponding to light polarized parallel to the plane of incidence on the tilted grating fringes, as shown in figure 1, i.e. P-polarized) couples to radially polarized cladding modes while x-polarized light (perpendicular to the tilt plane, or S-polarized) couples to

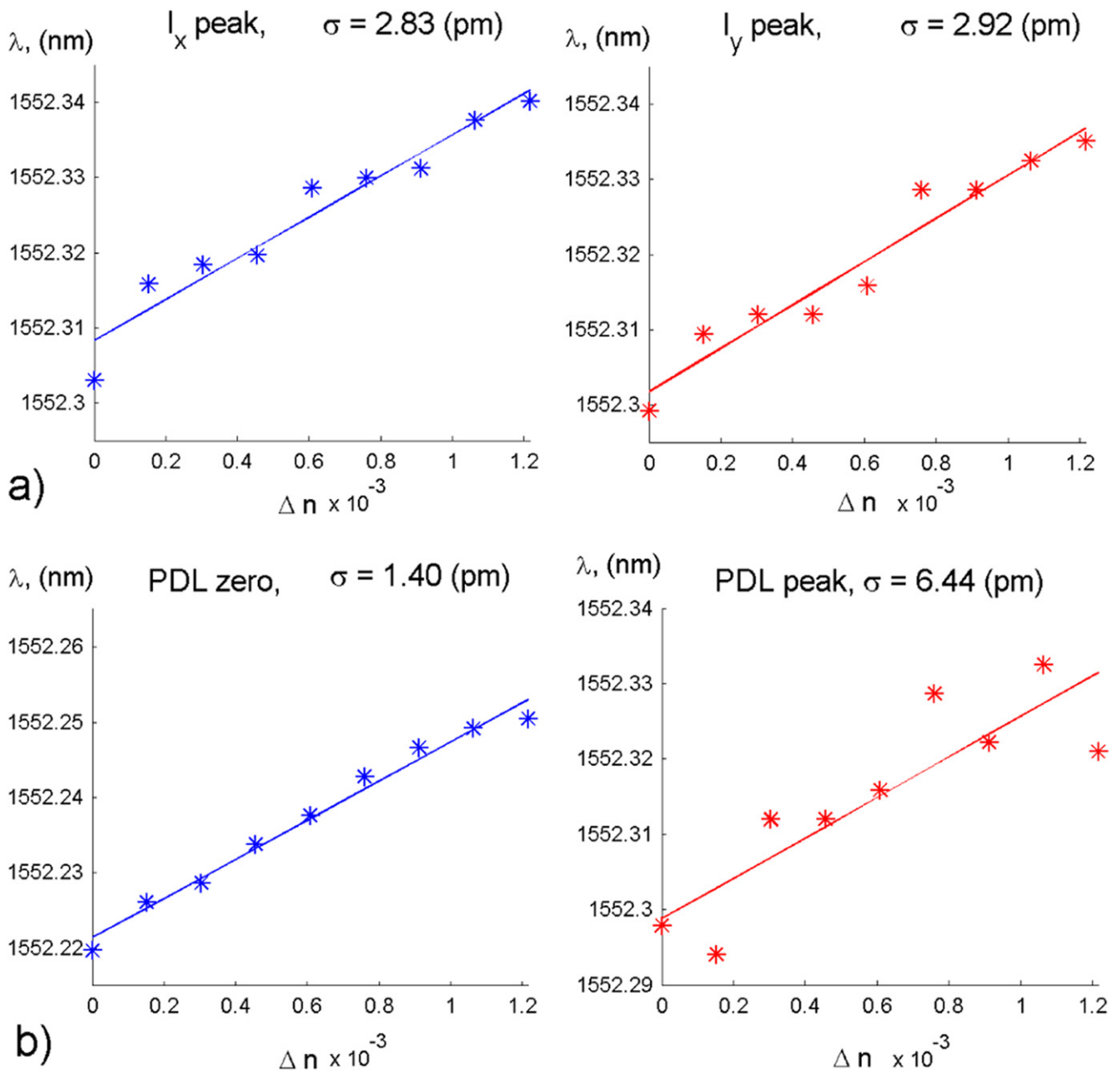


Figure 8. Position of the resonance (a) in the transmission spectra I_x and I_y of light polarized along \hat{x} and \hat{y} geometrical axes here aligned with the principal axes, and (b) in PDL spectra (the maximum and zero values of PDL are detected), as a function of refractive index change. The continuous lines represent the least square approximation to the measured data, and SD is the standard deviation from the linear approximation.

azimuthally polarized cladding modes (tangential to the boundary). Further polarization effects arise with non-uniform metal coatings, since they have boundaries that are both tangential and radially oriented relative to the cylindrical geometry of the fiber [21]. It is therefore desirable to carry out two transmission measurements along the principal axis to observe directly such polarization effects on the strengths and positions of the cladding mode resonances [22]. On the other hand, it has been shown here that a Jones matrix measurement can provide this information as well, in addition to other parameters of interest, such as PDL. While the PDL spectrum ‘hides’ the physical effects responsible for difference in

transmission due to the different polarization states, it has been shown in the past to yield excellent limits of detection for surface plasmon resonance based TFBG sensors [6]. We now proceed to compare the signal noise for refractive index measurements by the various polarization dependent data extraction techniques.

As shown in figure 7 for a TFBG coated with a sparse layer of gold nanorods and immersed in water, the PDL parameter provides the absolute value of the difference between resonances observed in the transmission spectra measured along the principal axes. The relative position of the peaks, their amplitude, and their width become convoluted in

the PDL parameter, which provides instead a maximum located somewhat in between the individual resonance maxima and a zero on either side corresponding to the wavelengths where the spectra cross each other. When the refractive index of the medium surrounding such TFBG changes the waveguiding characteristics of the cladding are modified and the resonances observed in the transmission spectrum change accordingly. Therefore, to detect changes in refractive index we can either follow the amplitudes and positions of individual resonances [22] or of the PDL features. Here, the sensor was immersed in water and the refractive index was incrementally increased in steps of $\Delta n = 1.517 \times 10^{-4}$ by adding each time 10 μl of ethylene glycol ($\text{C}_2\text{H}_4(\text{OH})_2$) to the 5 ml volume of water in which the grating was immersed. The impact of each increase in refractive index on all parameters of interest is shown in figure 8 for a typical slice of the spectrum (it was noted in [8] that there was little difference in wavelength shifts across the TFBG spectrum for this device).

The refractive index change was chosen to have a relatively small value of ($\Delta n = 1.517 \times 10^{-4}$) to test the sensor detection limits and a linear fitting was used because the sensor response for such small changes is expected to be linear. The standard deviation of the errors from the linear fit was calculated in the usual manner by:

$$\text{SD} = \sqrt{\frac{1}{N} \sum_{i=1}^N (x_i - \mu)^2}, \quad (19)$$

here μ is the expected value of \vec{x} , and $\vec{x} = \vec{y}_{\text{appr}} - \vec{y}_{\text{data}}$ is the difference between the measured data \vec{y}_{data} and its linear approximation \vec{y}_{appr} .

The results of the fits show that the most accurate detection of the refractive index change is achieved with the zeros in the PDL spectrum, as this measurement provides the smallest standard deviation of $\text{SD} = 1.40$ pm. For information, the refractometric sensitivity of this particular device is 27 (+/1) nm/RIU. The worst result were obtained with the PDL peak ($\text{SD} = 6.44$ pm), while the detection of individual polarized resonances provides an intermediate value of the standard deviation (essentially equal to 3 pm). It is not surprising that zeros of PDL should provide the most accurate results as they consist essentially of a differential measurement between two spectra with well-defined crossing points that occur on the sides of the individual resonances, where the spectral slope is highest. On the other hand, at the expense of an increase in noise by a factor of approximately 2, other effects such as differences in the change in the resonance amplitude for the two polarizations (which can be linked to differential loss or scattering) can be studied when the principal axis spectra are used.

6. Conclusion

In this paper we investigated the use of Jones matrix and Stokes vector based techniques and polarization analysis to extract information from optical fiber sensors in non-

polarization maintaining fibers. In particular we showed how to calculate transmission spectra with electric fields \vec{E} aligned with the system principal axes or along any other system axes. In the case of a TFBG inscribed in a non-polarization maintaining fiber for instance, the principal axes of the system are determined by the direction of the tilt of the grating planes (and its perpendicular). The transmission spectra for light polarized in the tilt plane (P-polarized) or out of the tilt plane (S-polarized) can thus be extracted without having to separately align a linear polarizer upstream from the grating and hoping that the polarization remains linear between the polarizer and the TFBG. Polarization-resolved spectra can also be obtained at a faster rate, for applications in chemical deposition process monitoring for instance, without the need to line up or rotate a polarizer between each measurement.

The transmission spectra of P- and S-polarized light were compared with the TFBG spectral response along the principal axes. A small oscillation of about 8° in the orientation of the principal axes as a function of wavelength was observed.

Furthermore, it was determined that the best TFBG sensor detection limits are achieved when zeros in the PDL spectrum are followed, mainly because of the sharpness of crossing points occurring on the steep sides of the individual resonances, but at the expense of the direct observation of the sensor response to polarized light (which are also available from the Jones matrix data). In the latter case, while the standard deviation of the spectral sensitivity is doubled relative to PDL measurements, additional information becomes available regarding the influence of the measured medium on cladding mode loss, allowing further uses of the TFBG data sets [23].

References

- [1] Zhang M, Ihida-Stansbury K, der Spiegel J V and Engheta N 2012 Polarization-based non-staining cell detection *Opt. Express* **20** 25378–90
- [2] Cranch G A, Flockhart G M H and Kirkendall C K 2006 Polarization properties of interferometrically interrogated fiber bragg grating and tandem-interferometer strain sensors *J. Lightwave Technol.* **24** 1787
- [3] Kotov O, Kol'chenko M and Lozovik Y E 2013 Ultrahigh refractive index sensitivity of te-polarized electromagnetic waves in graphene at the interface between two dielectric media *Opt. Express* **21** 13533–46
- [4] Wang R, Du L, Zhang C, Man Z, Wang Y, Wei S, Min C, Zhu S and Yuan X-C 2013 Plasmonic petal-shaped beam for microscopic phase-sensitive spr biosensor with ultrahigh sensitivity *Opt. Lett.* **38** 4770–3
- [5] Albert J, Shao L-Y and Caucheteur C 2013 Tilted fiber Bragg grating sensors *Laser Photonics Rev.* **7** 83–108
- [6] Caucheteur C, Shevchenko Y, Shao L-Y, Wuilpart M and Albert J 2011 High resolution interrogation of tilted fiber grating spr sensors from polarization properties measurement *Opt. Express* **19** 1656–64
- [7] Caucheteur C, Bette S, Chen C, Wuilpart M, Megret P and Albert J 2008 Tilted fiber bragg grating refractometer using polarization-dependent loss measurement *IEEE Photonics Technol. Lett.* **20** 2153–5

- [8] Bialiyeyu A, Bottomley A, Prezgot D, Ianoul A and Albert J 2012 Plasmon-enhanced refractometry using silver nanowire coatings on tilted fibre bragg gratings *Nanotechnology* **23** 444012
- [9] Smith A M 1978 Polarization and magneto-optic properties of single-mode optical fiber *Appl. Opt.* **17** 52–56
- [10] Alam M Z and Albert J 2013 Selective excitation of radially and azimuthally polarized optical fiber cladding modes *J. Lightwave Technol.* **31** 3167–75
- [11] Lee K S and Erdogan T 2000 Fiber mode coupling in transmissive and reflective tilted fiber gratings *Appl. Opt.* **39** 1394–404
- [12] Thomas J, Jovanovic N, Becker R G, Marshall G D, Withford M J, Tünnermann A, Nolte S and Steel M J 2011 Cladding mode coupling in highly localized fiber bragg gratings: modal properties and transmission spectra *Opt. Express* **19** 325–41
- [13] Villanueva G E, Jakubinek M B, Simard B, Oton C J, Matres J, Shao L-Y, Pérez-Millán P and Albert J 2011 Linear and nonlinear optical properties of carbon nanotube-coated single-mode optical fiber gratings *Opt. Lett.* **36** 2104–6
- [14] Chow K K, Tsuji M and Yamashita S 2010 Single-walled carbon-nanotube-deposited tapered fiber for four-wave mixing based wavelength conversion *Appl. Phys. Lett.* **96** 061104
- [15] Bialiyeyu A, Caucheteur C, Ahamad N, Ianoul A and Albert J 2011 Self-optimized metal coatings for fiber plasmonics by electroless deposition *Opt. Express* **19** 18742–53
- [16] Jones R C 1941 A new calculus for the treatment of optical systems *J. Opt. Soc. Am.* **31** 488–93
- [17] Heffner B L 1992 Deterministic, analytically complete measurement of polarization-dependent transmission through optical devices *IEEE Photonics Technol. Lett.* **4** 451–4
- [18] Berry H G, Gabrielse G and Livingston A E 1977 Measurement of the Stokes parameters of light *Appl. Opt.* **16** 3200–5
- [19] Goldstein D H 1992 *Polarized Light Revised and Expanded* (Boca Raton, FL: CRC Press)
- [20] McMaster W H 1954 Polarization and the Stokes parameters *Am. J. Phys.* **22** 351–62
- [21] Zhou W, Mandia D J, Griffiths M B, Bialiyeyu A, Zhang Y, Gordon P G, Barry S T and Albert J 2013 Polarization-dependent properties of the cladding modes of a single mode fiber covered with gold nanoparticles *Opt. Express* **21** 245–55
- [22] Caucheteur C, Chen C, Voisin V, Berini P and Albert J 2011 A thin metal sheath lifts the degeneracy in the cladding mode refractometric sensitivity of optical fiber sensors *Appl. Phys. Lett.* **99** 041118
- [23] Zhou W, Mandia D J, Griffiths M B E, Barry S T and Albert J 2014 Effective permittivity of ultrathin chemical vapor deposited gold films on optical fibers at infrared wavelengths, *J. Phys. Chem. C* **118** 670–8